IN-24
14944
p 24

NASA Technical Memorandum 104354

Combined Thermal and Bending Fatigue of High-Temperature Metal-Matrix Composites: Computational Simulation

Pascal K. Gotsis
Lewis Research Center
Cleveland, Ohio

June 1991

NASA

COMBINED THERMAL AND BENDING FATIGUE OF HIGH-TEMPERATURE METAL-MATRIX COMPOSITES: COMPUTATIONAL SIMULATION

Pascal K. Gotsis
National Aeronautics and Space Administration
Lewis Research Center
Cleveland, Ohio 44135

SUMMARY

The nonlinear behavior of a high-temperature metal-matrix composite (HT-MMC) was simulated by using the METCAN (Metal Matrix Composite Analyzer) computer code. The simulation started with the fabrication process, proceeded to thermomechanical cyclic loading, and ended with the application of a monotonic load. Classical laminate theory and composite micromechanics and macromechanics are used in METCAN, along with a multifactor interaction model for the constituents' behavior. The simulation of the stress-strain behavior from the macromechanical and the micromechanical points of view, as well as the initiation and final failure of the constituents and the plies in the composite, was examined in detail. It was shown that, when the fibers and the matrix were perfectly bonded, the fracture started in the matrix and then propagated with increasing load to the fibers. After the fibers fractured, the composite lost its capacity to carry additional load and fractured.

INTRODUCTION

High-temperature metal-matrix composites HT-MMC's have significant potential payoffs when used in hot structural components of advanced aerospace propulsion systems. Realization of these payoffs depends on the development of the following: (1) fabrication technology, (2) experimental techniques for measuring composite thermal and mechanical characterisitc properties, and (3) computational simulations that predict the nonlinear behavior of HT-MMC's.

At NASA Lewis Research Center a computer program called METCAN (Metal Matrix Composite Analyzer) is being developed (refs. 1 to 6) to simulate the nonlinear behavior of HT-MMC's from the constituent material level to the laminate level. The simulation capability of METCAN is shown in figure 1. The micromechanical constitutive equations used to simulate the nonlinear thermomechanical behavior of HT-MMC's consist of products of terms with unknown exponents, as shown in figure 2. The exponents are determined for the specific material and type of nonlinear dependence. They are determined from experimental data (if available) or are estimated from the anticipated intuitive behavior of the particular term.

Although METCAN is continually used to simulate HT-MMC behavior, it had not yet been used to simulate the nonlinear behavior of HT-MMC laminates subjected to cyclic bending.

This report describes the computational simulation of the nonlinear behavior of an HT-MMC laminate subjected first to thermomechanical cyclic bending and later to monotonic loading. The monotonic load was increased gradually until the composite fractured. The simulation procedure is described in some detail. The initiation of local fracture and its propagation within the laminate were examined. The results obtained are summarized and discussed in order to demonstrate the potential capabilities of METCAN in these types of simulations.

COMPUTATIONAL SIMULATION

The HT-MMC consisted of three plies with orientation 0°/90°/0°. The thickness of the 0° plies was 0.05 in., and the thickness of the 90° ply was 0.10 in. The composite consisted of silicon carbide (SiC) fibers with a fiber volume ratio of 40 percent in a Ti-15-3 matrix. The material properties of the Ti-15-3 and of the SiC were taken from the data bank available in METCAN and are shown in table I. The fibers were continuous and were assumed to be perfectly bonded to the matrix at the interface. The computer code can compute the temperature dependence of constituent properties at any temperature; the material properties of the composite constituents were given at room temperature. In addition METCAN can compute the global

properties at a laminate level by using macromechanics and the local properties at the ply level by using micromechanics. The simulation steps are shown in figures 3 and 13 and are described here.

Fabrication Process

The composite was subjected to a high temperature (T_c = 1750 °F, close to the matrix consolidation temperature of 1800 °F) and gradually cooled to room temperature ($0.04T_c$ = 70 °F).

Combined Cyclic Thermal and Bending Loads

The applied thermal cycles were 75 percent of the default allowable thermal cycles (N_{tf} = 400 cycles) in METCAN. The applied mechanical (bending) cycles were 1 percent of the default allowable mechanical cycles ($N_{mf} = 10^4$ cycles) in METCAN. Both the uniaxial tensile and bending loads were applied simultaneously.

Monotonic Load

Two different types of monotonic loads were applied and examined separately. In the first case a uniaxial tensile load N_{xx} was applied along the 0° ply direction (fig. 3). The applied load was increased slowly until the composite failed at 44 percent of the ultimate load N_u (26 000 lb/in. = $\sigma_{mat}^{ult}\, t$, where σ_{mat}^{ult} is the tensile allowable strength of the matrix at room temperature and t is the thickness of the laminate). In the second case a pure bending load M_{xx} was applied (fig. 13). The bending load was increased slowly until the composite failed at 95 percent of the M_u value (M_u = 866.67 lb in./in. = $\sigma_{mat}^{ult}\, t^2/6$, where σ_{mat}^{ult} and t were defined above).

Note that local failure was defined as when the local constituent stress exceeded the fracture stress for that constituent (maximum stress criterion).

Values of the exponents that are used in the multifactor interaction relationship (fig. 2) were computed from the constituent experimental data whenever possible. If data were not available, default values obtained from studies conducted on other metal-matrix composites were used. The default values of the exponents for the constituent materials that were used are shown in table II.

RESULTS AND DISCUSSION

The following results refer to the stage where the monotonic load was applied and increased slowly until the composite failed. This was after the laminate had been subjected to the fabrication process and thermomechanical cyclic loading.

Uniaxial Tensile Load

The laminated composite that was subjected to monotonic uniaxial tensile loading with the structural coordinates x, y, and z and a single fiber with the surrounding matrix and the material coordinates 1, 2, and 3 are shown in figure 3. Note that the figure shows equal thicknesses for the three plies although the middle ply was twice as thick as the top and bottom plies.

Evolution of fracture in composite.—Prior to monotonic uniaxial loading the thermomechanical cyclic load was applied. At the end of thermomechanical cyclic loading the bottom (0°) ply fractured in the transverse direction within the matrix in region A. When the monotonic uniaxial tensile load N_{xx} was applied and the stress ratio

$$\frac{N_{xx}}{(\text{Composite thickness})(\text{Matrix tensile strength})}$$

reached 0.11, the middle (90°) ply fractured in the longitudinal direction within the matrix in region A. At a stress ratio of 0.15 the bottom (0°) ply fractured in the longitudinal direction within the matrix in regions A and C. When the stress ratio was increased to 0.36, the top (0°) ply fractured in the longitudinal direction within the matrix in regions A and C. At a stress ratio of 0.37 the middle (90°) ply fractured in the transverse direction within the matrix in region C. Finally, when the stress ratio reached 0.44 high longitudinal stresses developed in the middle (90°) ply within the matrix in regions A and C and fracture occurred. Also the fibers broke in the bottom (0°) ply in the longitudinal direction because stresses exceeding the fracture stress of the fibers developed when the surrounding matrix broke and the entire applied load was transferred to the fibers. The composite then fractured because it could not carry any additional load.

The evolution of the fracture that took place in the composite due to the uniaxial load is shown in tables III and IV for the matrix and the fibers, respectively. Note that the results shown in the tables are referred to the material coordinates 1, 2, and 3.

Stress-strain behavior of composite, plies, and constituent materials.—The stress-strain behavior of the composite under tensile loading is shown in figure 4. The failure modes of the composite at applied stress ratios of 0.11, 0.15, 0.36, 0.37, and 0.44 are shown in figure 3 and correspond to the points M1, M2, M3, M4, and Failure, respectively, in figure 4. When the stress ratio reached 0.44, the constituent materials failed and the composite fractured.

Longitudinal behavior of top (0°) ply: The longitudinal stress-strain behavior of the top (0°) ply, as well as of its constituent fiber and matrix, is shown in figure 5. At the indicated point M3 (fig. 5(a)) at a stress ratio of 0.36 the matrix fractured in the top ply in the longitudinal direction in regions A and C; and at a stress ratio of 0.44 (failure point) the ply fractured.

At the indicated failure point the developed longitudinal ply stresses were equal to 98.46 ksi, much greater than the allowable tensile strength of 74.69 ksi. The linear stress-strain behavior of the fiber is shown in figure 5(b). At an applied stress ratio of 0.44 the developed longitudinal stresses were equal to 181 ksi, less than the allowable tensile strength of 186.7 ksi. Note that the fiber longitudinal modulus, which is the slope of the curve in figure 5(b), was lower than the corresponding modulus at room temperature (reference input data). The reason is that the number of thermocycles (300 cycles of input data) was 75 percent of the default ultimate number of thermal cycles assumed in METCAN. This contributed to rapid degradation of the mechanical properties of the constituent fiber and matrix, lowering the moduli of the constituents.

The linear stress-strain behavior of the matrix for both regions A and C is shown in figure 5(c). At a stress ratio of 0.36 (point M3) the matrix fractured. At the indicated point M3 the developed longitudinal stresses were a little greater than the allowable tensile strength of 43.17 ksi.

Transverse behavior of top (0°) ply: The transverse stress-strain behavior of this 0° ply, as well as of its constituent fiber and matrix, is shown in figure 6. The stress-strain behavior of the top ply (fig. 6(a)) was nonlinear. When the applied stress ratio reached 0.44, the developed stresses were 7.6 ksi, less than the allowable tensile stength of 12.3 ksi. The stress-strain behavior of the fiber (fig. 6(b)) was linear. When the applied stress ratio reached 0.44, the developed stresses were much lower than the allowable compressive strength of 242.7 ksi. The matrix microstresses were linear in region A (fig. 6(c)). At a stress ratio of 0.44 the developed stresses were 37 ksi, less than the allowable tensile strength of 42.95 ksi. The stress-strain relation of the matrix was linear in region C (fig. 6(d)). At a stress ratio of 0.44 the developed compressive stresses were 12 ksi, less than the allowable compressive strength of 42.95 ksi.

Longitudinal behavior of middle (90°) ply: The longitudinal stress-strain behavior of the middle (90°) ply, as well as of its consituent fiber and matrix, is shown in figure 7. The ply stress-strain behavior was nonlinear (fig. 7(a)). At a stress ratio of 0.37 the middle ply fractured in the transverse direction within the matrix in region C. At an applied stress ratio of 0.44 the developed compressive stresses were 6.5 ksi, less than the allowable compressive strength of 47.54 ksi. The fiber stress-strain behavior was linear (fig. 7(b)). At a stress ratio of 0.44 the developed compressive stresses were 213 ksi, less than the allowable compressive strength of 223.6 ksi. The matrix stess-strain behavior for both regions A and C is shown in figure 7(c). At a stress ratio of 0.44 the developed microstresses were 32.7 ksi, less than the allowable strength of 39.7 ksi.

Transverse stress-strain behavior of middle (90°) ply: The transverse stress-strain behavior of the 90° ply and its constituent fiber and matrix are shown in figure 8. The ply stress-strain behavior was nonlinear (fig. 8(a)). At the indicated point M4 at a stress ratio of 0.37 the matrix fractured in the transverse direction in region C, and at the failure point at a stress ratio of 0.44 the ply fractured. The developed stresses of 28.2 ksi were greater than the tensile strength of 11.32 ksi. The linear stress-strain

behavior of the fiber is shown in figure 8(b). At a stress ratio of 0.44 the developed stresses were 39.6 ksi, less than the allowable strength of 171.9 ksi. The matrix stress-strain behavior at region A was linear (fig. 8(c)). Fracture occurred at the indicated point M1 when the stress ratio was 0.11. The developed stresses were slightly higher than the allowable strength of 40.21 ksi. The stress-strain behavior of the matrix in region C was also linear (fig. 8(d)). Failure occurred at the indicated point M4. The developed stresses of 45 ksi were greater than the allowable strength of 39.7 ksi.

Longitudinal behavior of bottom (0°) ply: The longitudinal stress-strain behavior of this 0° ply, as well as of its constituent fiber and matrix, is shown in figure 9. The ply stress-strain behavior was nonlinear (fig. 9(a)). At an applied stress ratio of 0.44 the developed stresses were 76.2 ksi, less than the allowable strength of 143.4 ksi. The fiber stress-strain behavior was linear (fig. 9(b)). The fiber failed at a stress ratio of 0.44 (failure point). The developed microstresses slightly exceeded the allowable strength of 143.4 ksi. The matrix stress-strain behavior for both regions A and C was linear (fig. 9(c)). The matrix failed at a stress ratio of 0.37 (point M4). The developed stresses of 33.21 ksi were slightly greater than the allowable strength of 33.15 ksi.

Transverse stress-strain behavior of bottom (0°) ply: The transverse stress-strain behavior of this 0° ply, as well as of its constituent fiber and matrix, is shown in figure 10. The ply stress-strain behavior was nonlinear (fig. 10(a)). At a stress ratio of 0.44 the developed stresses were 7.36 ksi, less than the allowable strength of 9.45 ksi. The fiber stress-strain behavior was linear (fig. 10(b)). At a stress ratio of 0.44 the developed compressive stresses were 11 ksi, less than the allowable compressive strength of 186.5 ksi. The stress-strain behavior of the matrix in region C was also linear (fig. 10(c)). At an applied stress of 0.44 the developed compressive stresses were 10.8 ksi, less than the allowable compressive strength of 33 ksi. The stress-strain behavior of the matrix in region A is not shown because premature fracture occurred in this region prior to monotonic tensile loading.

Influence of loading history on allowable strength of ply and its constituents.—The effect of processing, thermocycling, and monotonic tensile loading on the allowable strength is shown in figures 11 and 12. The allowable strengths in the longitudinal and transverse directions for the different plies (top, middle, and bottom) are shown in figure 11. The allowable fiber and matrix strengths in the longitudinal direction for the different plies (top, middle, and bottom) are shown in figure 12. The most severe type of loading was thermocycling. It is responsible for the strength degradation, because the applied number of thermal cycles was very high, equal to 75 percent of the allowable by default in METCAN.

Bending Load

Evolution of fracture in composite.—Prior to monotonic bending loading the thermomechanical load was applied (fig. 13), and local fracture began in the transverse direction within the matrix of the bottom ply, in region A. When the monotonic bending load M_{xx} was applied and the moment ratio M_{xx}/M, where

$$M = \frac{(\text{Matrix tensile strength})(\text{Composite thickness})^2}{6}$$

was 0.26, local fracture occurred in the longitudinal direction within the matrix of the bottom ply in regions A and C. When the moment ratio was 0.95, the fibers fractured in the longitudinal direction in the top and bottom plies. Then the composite fractured because it could not carry any additional load.

The evolution of the fracture that took place in the composite due to the quasi-static bending load is shown in tables V and VI for the matrix and fibers, respectively. Note that the results shown in the tables are referred to the material coordinates 1, 2, and 3 but the evolution of the fracture in the composite is referred to the global coordinates x, y, and z.

Stress-strain behavior of plies and constituent materials.—The behavior of the developed bending moment versus the curvature in the x direction of the composite is shown in figure 14. The indicated points M1, M2, M3, and Failure correspond to applied moment ratios of 0.26, 0.85, 0.90, and 0.95, respectively. When the stress ratio reached 0.95, the composite fractured.

Top (0°) ply: The longitudinal stress-strain behavior of this 0° ply and of its constituent fiber and matrix is shown in figure 15; and transverse stress-strain behavior, in figure 16. The stress-strain behavior of the ply was linear (fig. 15(a)). At a

moment ratio of 0.95 the ply developed compressive stresses of 107.1 ksi, greater than the allowable compressive strength of 26.02 ksi and fractured (failure point in fig. 15(b)). The fiber stress-strain behavior was linear (fig. 15(b)). At the indicated failure point at a moment ratio of 0.95 the fiber fractured because the developed fiber compressive stresses of 243 ksi were greater than the allowable compressive strength of 242.3 ksi. The matrix stress-strain behavior in both regions A and C was linear (fig. 15(c)). At a moment ratio of 0.95 the developed matrix compressive stresses were 40 ksi, less than the allowable compressive strength of 43.3 ksi.

The transverse stress-strain behavior of the top (0°) ply and its constituents is shown in figure 16. The stress-strain behavior of the ply was linear (fig. 16(a)). At a moment ratio of 0.95 the developed stresses in the ply were 4.3 ksi, less than the allowable strength of 12.4 ksi. The fiber stress-strain behavior was also linear (fig. 16(b)). At a moment ratio of 0.95 the developed compressive stresses were 14 ksi, much less than the allowable compressive strength of 243 ksi. The stress-strain behavior of the matrix in region A was linear (fig. 16(c)). At a moment ratio of 0.95 the developed stresses in the matrix were 34 ksi, less than the allowable strength of 43.3 ksi. The matrix stress-strain behavior in region C was linear (fig. 16(d)). At a moment ratio of 0.95 the developed compressive stresses in region C were equal to 14 ksi, less than the allowable compressive strength of 43 ksi.

Middle (90°) ply: The longitudinal stress-strain behavior of the middle ply and its constituents is shown in figure 17. The stress-strain behavior of the ply was nonlinear (fig. 17(a)). At the indicated point M1 (moment ratio, 0.26) the matrix failed in both regions A and C in the bottom ply. At the indicated point M2 the moment ratio was 0.86. When the moment ratio reached 0.95, the developed compressive stresses in the ply were 5.2 ksi, much less than the allowable compressive strength of 47.9 ksi. The stress-strain behavior of the fiber was linear (fig. 17(b)). At a moment ratio of 0.95 the developed compressive stresses in the fiber were 52.9 ksi, much less than the allowable compressive strength of 223.6 ksi. The matrix stress-strain behavior was linear for both regions A and C (fig. 17(c)). When the moment ratio reached 0.95, the developed stresses in the matrix were 27.5, less than the allowable strength of 40 ksi.

The transverse stress-strain behavior of the middle (90°) ply and its constituents is shown in figure 18. The ply had linear stress-strain behavior (fig. 18(a)). When the moment ratio reached 0.95, the developed ply stresses (13.6 ksi) were greater than the allowable ply strength (11.43 ksi) and failure occurred. The fiber had linear stress-strain behavior (fig. 18(b)). At a moment ratio of 0.95 the developed fiber stresses (~19.4 ksi) almost equaled the allowable fiber strength (19.4 ksi). The matrix stress-strain behavior was linear in both regions A (fig. 18(c)) and C (fig. 18(d)). At a moment ratio of 0.95 the developed stresses in both regions were less than the allowable strength (39.9 ksi).

Bottom (0°) ply: The longitudinal stress-strain behavior of the bottom ply and its constituents is shown in figure 19. The stress-strain behavior of the ply was nonlinear (fig. 19(a)). At a stress ratio of 0.95 the developed ply stresses (77 ksi) were less than the allowable strength (143.5 ksi). The fiber stress-strain behavior was linear (fig. 19(b)). At a moment ratio of 0.95 the developed fiber stresses (143.8 ksi) were slightly higher than the allowable strength (143.5 ksi) and the fiber fractured. The stress-strain behavior of the matrix in regions A and C was linear (fig. 19(c)). At the indicated point M1 (moment ratio, 0.26) the developed stresses (33.7 ksi) in the matrix were slightly higher than the allowable strength (33.6 ksi) and failure occurred.

The transverse stress-strain behavior for the bottom (0°) ply and its constituents is shown in figure 20. The stress-strain behavior of the ply was nonlinear (fig. 20(a)). At a moment ratio of 0.95 the developed ply stresses (6.03 ksi) were less than the allowable strength (9.5 ksi). The fiber stress-strain behavior was linear (fig. 20(b)). At a moment ratio of 0.95 the developed fiber compressive stresses (11.2 ksi) were much less than the allowable compressive strength (186.6 ksi). The stress-strain behavior of the matrix in region C was also linear (fig. 20(c)). At a moment ratio of 0.95 the developed compressive stresses in the matrix (11.1 ksi) were less than the allowable compressive strength (33 ksi).

Influence of loading history on allowable strength of ply and its constituents.—The effect of processing, thermocycling, and monotonic tensile loading on the allowable strength is shown in figures 21 and 22. The most severe type of loading is thermocycling. It is responsible for the strength degradation because the applied number of thermal cycles were very high, equal to 75 percent of the allowable by default in METCAN.

The allowable strengths in the longitudinal and transverse directions for the different plies (top, middle, and bottom) are shown in figure 21. The allowable strength in the longitudinal direction for the constituents is shown in figure 22.

CONCLUSIONS

The nonlinear behavior of a metal-matrix composite subjected to the fabrication process, to combined cyclic thermal and bending loading, and finally to a monotonic load to fracture was simulated computationally by METCAN.

The stress-strain behavior of the composite and its constituents was simulated from the micromechanical and macromechanical points of view. It was shown that the behavior of the composite, the initiation of fracture, and the final failure of the composite depended on the type of loading that was applied on the composite. Under both types of loading (uniaxial tensile and bending loading) failure started in the matrices of the different plies and propagated to the fibers. When the fibers fractured, the composite lost its strength and fractured.

Thermomechanical cycling severely degraded the constituents' properties.

Finally, it was shown that the sequence/hierarchy of fracture modes can be identified in composite laminates subjected to different types of loading.

APPENDIX—SYMBOLS

C	heat capacity
E	modulus of elasticity
G	shear modulus
K	heat conductivity
M_{xx}	bending moment per unit width
N_{xx}	uniaxial tensile force per unit width
P	property
p	pressure
S_{iiC}	strength in compression in i direction, where i = 1,2
S_{iiT}	strength in tension in i direction, where i = 1,2
S_{1KS}	strength in shear in 1k plane, where k = 2,3
T	temperature
T_m	melting temperature
t	time constant
x, y, z	global coordinate system axes
1, 2, 3	composite material coordinate system axes
α_{ii}	coefficient of thermal expansion in i direction, where i = 1,2
σ_{iiA}, σ_{iiC}	normal microstresses in i direction, where i = 1,2 in the regions A and C, respectively, in matrix
σ_{ii}	normal microstresses in i direction, where i = 1,2,3 in fiber
ν_{1i}	Poisson's ratio in 1i direction, where i = 2,3

REFERENCES

1. Chamis, C.C., et al.: METCAN Verification Status. NASA TM-103119, 1990.
2. Hopkins, D.A.; and Chamis, C.C.: A Unique Set of Micromechanics Equations for High Temperature Metal Matrix Composites. NASA TM-87154, 1985.
3. Chamis, C.C.; and Hopkins, D.A.: Thermoviscoplastic Nonlinear Constitutive Relationships for Structural Analysis of High Temperature Metal Matrix Composites. NASA TM-87291, 1985.
4. Murthy, P.L.N.; Hopkins, D.A.; and Chamis, C.C.: Metal Matrix Composite Micromechanics: In Situ Behavior Influence on Composite Properties. NASA TM-102302, 1989.
5. Lee, H.-J.: METCAN Simulation of Candidate Metal Matrix Composites for High Temperature Applications. NASA TM-103636, 1990.
6. Lee, H.-J.; Murthy, P.L.N.; and Chamis, C.C.: METCAN Updates for High Temperature Composite Behavior: Simulation/ Verification. NASA TM-103682, 1991.

TABLE I.—FIBER AND MATRIX PROPERTIES AT ROOM TEMPERATURE

Property[a]	Fiber (SiC)	Matrix (Ti-15-3)
T_m, °F	4870.00	3000.00
E_{11}, Mpsi	62.00	12.30
E_{22}, Mpsi	62.00	12.30
ν_{12}, in./in.	0.30	0.32
ν_{13}, in./in.	0.30	0.32
G_{12}, Mpsi	23.80	4.66
G_{23}, Mpsi	23.80	4.66
α_{11}, ppm/°F	1.80	4.50
α_{22}, ppm/°F	1.80	4.50
K_{11}, Btu/hr in. °F	0.75	0.39
K_{22}, Btu/hr in. °F	0.75	0.39
C, Btu/lb	0.29	0.12
S_{11T}, ksi	500.00	130.00
S_{11C}, ksi	650.00	130.00
S_{22T}, ksi	500.00	130.00
S_{22C}, ksi	650.00	130.00
S_{12C}, ksi	300.00	91.00
S_{23C}, ksi	300.00	91.00

[a]See appendix for definitions.

TABLE II.—EXPONENTS FOR CONSTITUENT MATERIALS
[From multifactor interaction relationship (fig. 2).]

(a) Fiber

Property	Exponent					
	n	m	ℓ	p	q	r
Elastic modulus, E	0.25	0.25	0.25	0.50	0.50	0.50
Poisson's ratio, ν	0.25	0.25	0.25	0.50	0.50	0.50
Strength, S	0.25	0.00	0.25	0.50	0.50	0.50
Coefficient of thermal expansion, α	0.25	0.00	0.25	0.50	0.50	0.50
Heat conductivity, K	0.25	0.00	0.25	0.50	0.50	0.50

(b) Matrix

Property	Exponent					
	n	m	ℓ	p	q	r
Elastic modulus, E	0.50	0.50	0.50	0.50	0.50	0.50
Poisson's ratio, ν	0.50	0.50	0.50	0.50	0.50	0.50
Strength, S	0.50	0.00	0.50	0.50	0.50	0.50
Coefficient of thermal expansion, α	0.17	0.00	0.50	0.50	0.50	0.50
Heat conductivity, K	0.50	0.00	0.50	0.50	0.50	0.50

TABLE III.—EVOLUTION OF LOCAL FRACTURE IN MATRIX MATERIAL DUE TO UNIAXIAL TENSILE LOAD

Stress ratio	Ply number	Longitudinal direction[a]		Transverse direction[b]		Point on fig. 4
		σ_{11A}	σ_{11C}	σ_{22A}	σ_{22C}	
0.11	1	---	---	---	---	M1
	2	---	---	(c)	---	
	3	---	---	(d)	---	
0.15	1	---	---	---	---	M2
	2	---	---	(c)	---	
	3	(c)	(c)	(d)	---	
0.36	1	(c)	(c)	---	---	M3
	2	---	---	(c)	---	
	3	(c)	(c)	(d)	---	
0.37	1	(c)	(c)	---	---	M4
	2	---	---	(c)	(c)	
	3	(c)	(c)	(d)	---	
0.44	1	(c)	(c)	---	---	Failure
	2	(c)	(c)	(c)	(c)	
	3	(c)	(c)	(d)	---	

[a]σ_{11A} and σ_{11C} are the normal microstresses in the 1-direction (longitudinal direction) in regions A and C, respectively, in the matrix.

[b]σ_{22A} and σ_{22C} are the normal microstresses in the 2-direction (transverse direction) in regions A and C, respectively, in the matrix.

[c]Failure occurred in region A or C in the matrix.

[d]Failure occurred in the matrix prior to monotonic loading.

TABLE IV.—EVOLUTION OF LOCAL FRACTURE IN FIBER MATERIAL DUE TO UNIAXIAL LOAD

Stress ratio	Ply number	Uniaxial load[a]			Point on fig. 4
		σ_{11}	σ_{22}	σ_{33}	
0.44	1	---	---	---	Failure
	2	---	---	---	
	3	(b)	---	---	

[a]σ_{11},σ_{22}, and σ_{33} are the normal microstresses in the fiber in the directions 1-1, 2-2, and 3-3, respectively.

[b]Failure occurred in the fiber.

TABLE V.—EVOLUTION OF LOCAL FRACTURE IN MATRIX MATERIAL DUE TO QUASI-STATIC BENDING LOAD

Moment ratio	Ply number	Longitudinal direction[a]		Transverse direction[b]		Point on fig. 14
		σ_{11A}	σ_{11C}	σ_{22A}	σ_{22C}	
0.26	1	---	---	---	---	M1
	2	---	---	---	---	
	3	(c)	(c)	(d)	---	
0.86	1	---	---	---	---	M2
	2	---	---	---	---	
	3	(c)	(c)	(d)	---	
0.90	1	---	---	---	---	M3
	2	---	---	---	---	
	3	(c)	(c)	(d)	---	
0.95	1	---	---	---	---	Failure
	2	---	---	---	---	
	3	(c)	(c)	(d)	---	

[a]σ_{11A} and σ_{11C} are the normal microstresses in the 1-direction (longitudinal direction) in regions A and C, respectively, in the matrix.
[b]σ_{22A} and σ_{22C} are the normal microstresses in the 2-direction (transverse direction) in regions A and C, respectively, in the matrix.
[c]Failure occurred in region A or C in the matrix.
[d]Failure occurred in the matrix prior to monotonic loading.

TABLE VI.—EVOLUTION OF LOCAL FRACTURE IN FIBER MATERIAL DUE TO QUASI-STATIC BENDING LOAD

Moment ratio	Ply number	Bending load[a]			Point on fig. 14
		σ_{11}	σ_{22}	σ_{33}	
0.95	1	(b)	---	---	Failure
	2	---	---	---	
	3	(b)	---	---	

[a]σ_{11}, σ_{22}, and σ_{33} are the normal microstresses in the fiber in the directions 1-1, 2-2, and 3-3, respectively.
[b]Failure occurred in the fiber.

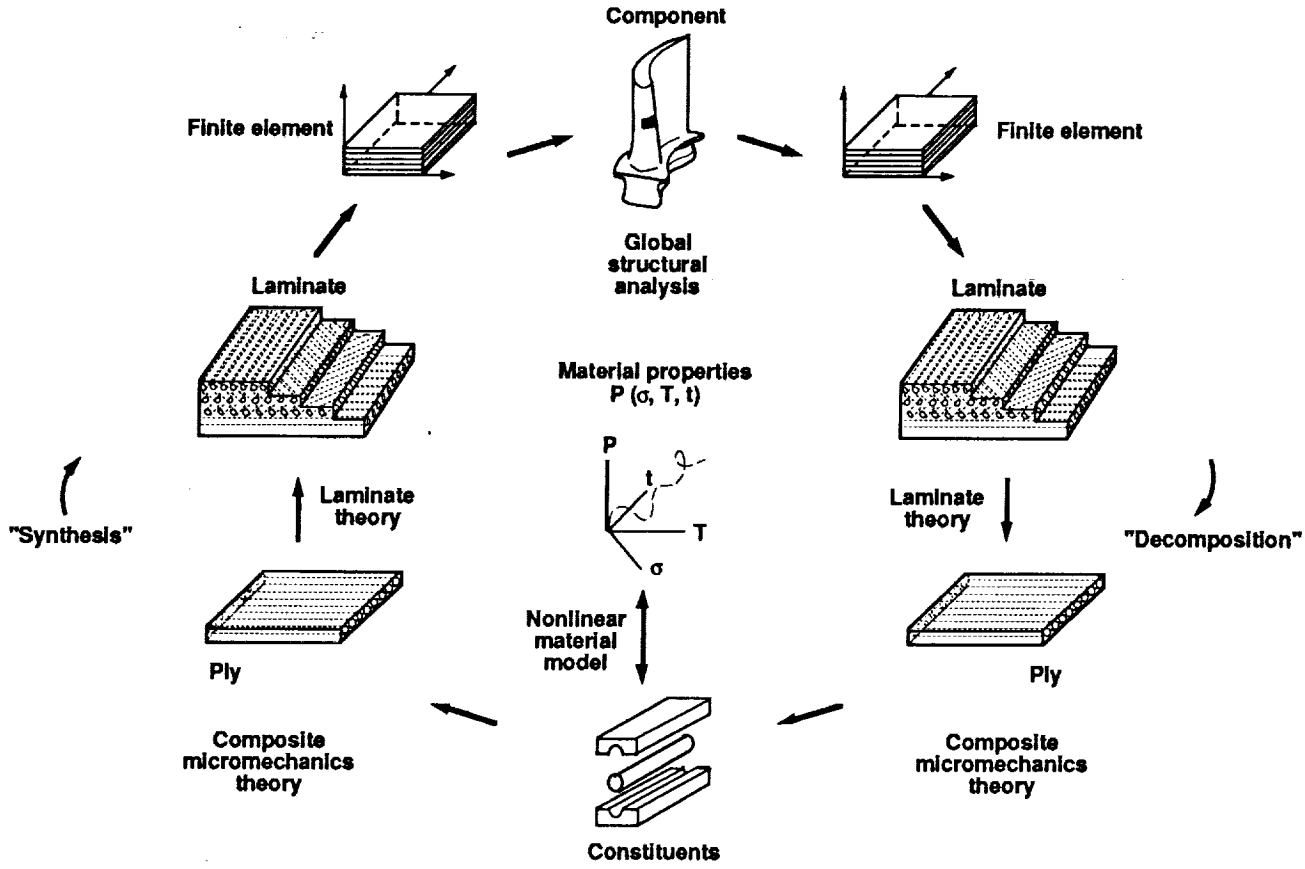

Figure 1.—Integrated approach to metal-matrix composite (MMC) analysis incorporated in METCAN.

$$\frac{P}{P_0} = \left(\frac{T_F - T}{T_F - T_0}\right)^n \left(\frac{S_F - \sigma}{S_F - \sigma_0}\right)^m \left(\frac{\dot{S}_F - \dot{\sigma}}{\dot{S}_F - \dot{\sigma}_0}\right)^l \left(\frac{\dot{T}_F - \dot{T}}{\dot{T}_F - \dot{T}_0}\right)^k \left(\frac{R_F - R}{R_F - R_0}\right)^p L$$

$$L \left(\frac{N_{MF} - N_M}{N_{MF} - N_{M0}}\right)^q \left(\frac{N_{TF} - N_T}{N_{TF} - N_{T0}}\right)^r \left(\frac{t_F - t}{t_F - t_0}\right)^s L$$

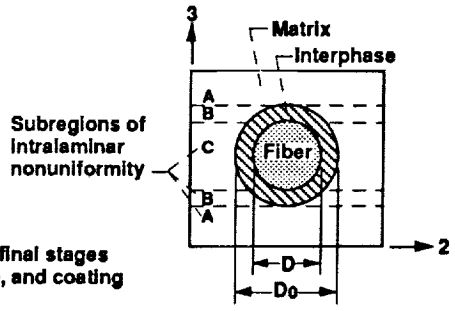

Rationale:

- Gradual effects during most of range, rapidly degrading near final stages
- Representative of in situ behavior for fiber, matrix, interphase, and coating
- Introduction of primitive variables (PV)
- Consistent in situ representation of all constituent properties in terms of PV
- Room-temperature values for reference properties
- Continuous interphase growth
- Simultaneous interaction of all primitive variables
- Adaptable to new materials
- Amenable to verification inclusive of all properties
- Readily adaptable to incremental computational simulation

Notations:

P – property; T – temperature; S – strength; R – metallurgical reaction; N – number of cycles; t – time; D – diameter; overdot – rate; subscripts: 0 – reference; F – final; M – mechanical; T – thermal

Figure 2.—Assumed multifactor interaction relationship to represent various factors that influence in situ constituent materials behavior.

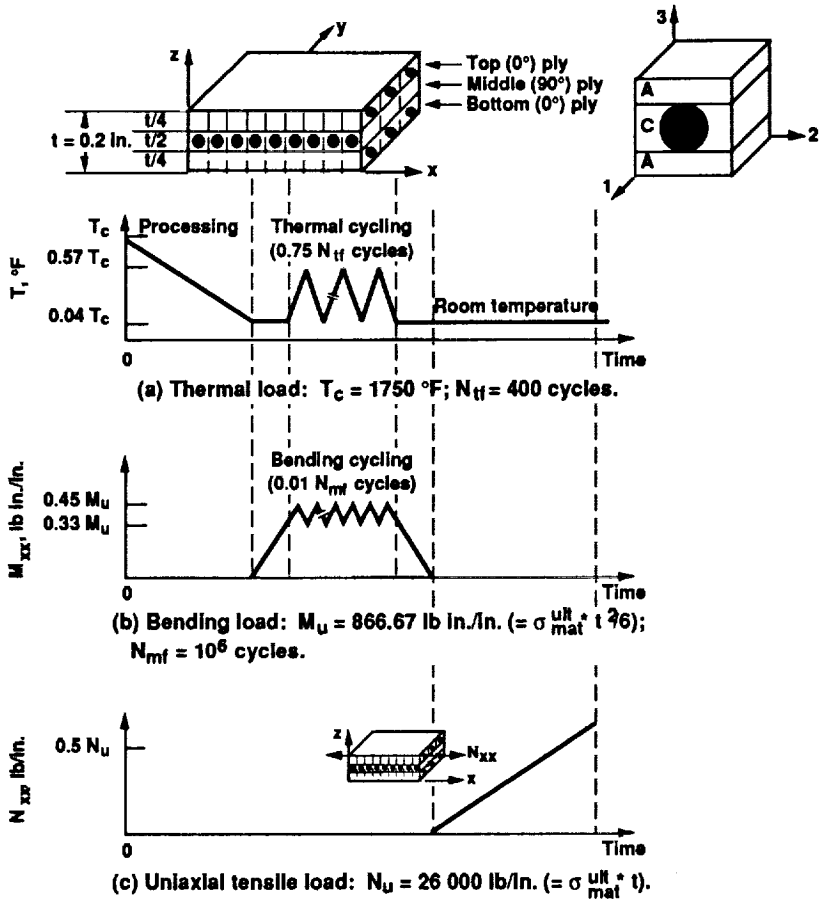

(a) Thermal load: T_c = 1750 °F; N_{tf} = 400 cycles.

(b) Bending load: M_u = 866.67 lb in./in. ($= \sigma_{mat}^{ult} * t^2/6$); $N_{mf} = 10^6$ cycles.

(c) Uniaxial tensile load: N_u = 26 000 lb/in. ($= \sigma_{mat}^{ult} * t$).

Figure 3.—First case of loading.

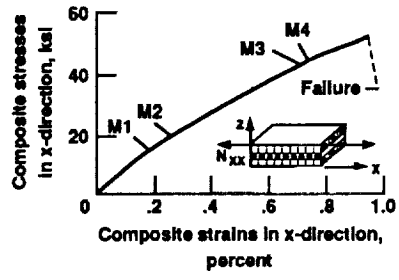

Figure 4.—Composite stress versus composite strain.

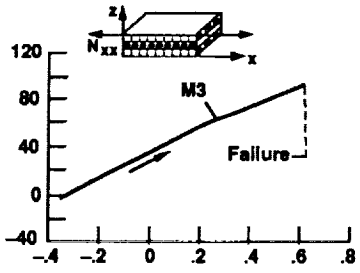

(a) Ply stresses.

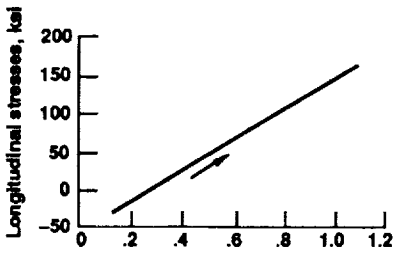

(b) Fiber microstresses.

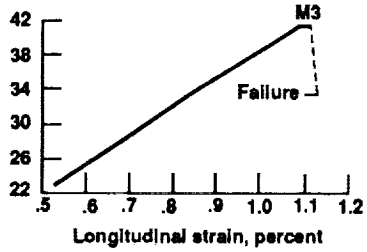

(c) Matrix microstresses at regions A and C.

Figure 5.—Longitudinal stress-strain curves for top (0°) ply and its fiber and matrix (region A).

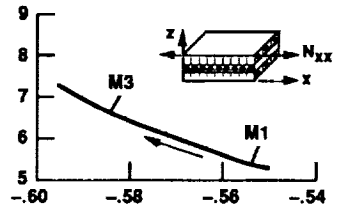

(a) Ply stresses.

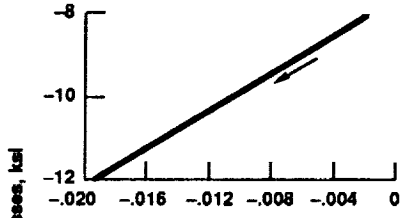

(b) Fiber microstresses.

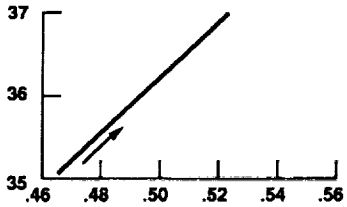

(c) Matrix microstresses in region A.

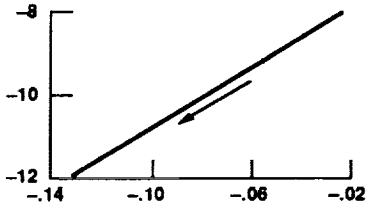

(d) Matrix microstresses in region C.

Figure 6.—Transverse stress-strain curves for top (0°) ply and its fiber and matrix (regions A and C).

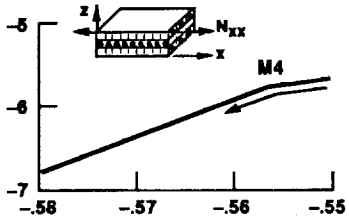

(a) Ply stresses.

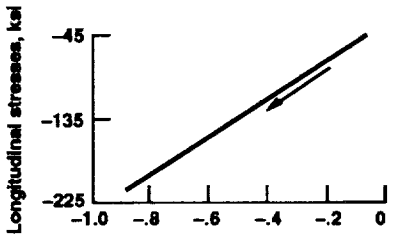

(b) Fiber microstresses.

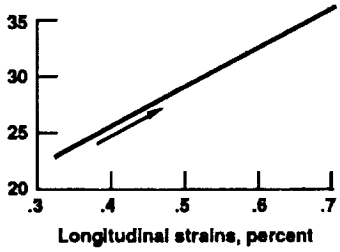

(c) Matrix microstresses in regions A and C.

Figure 7.—Longitudinal stress-strain curves for middle (90°) ply and its fiber and matrix (regions A and C).

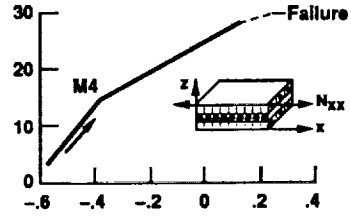

(a) Ply stresses.

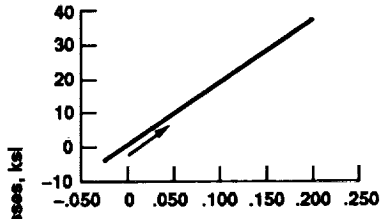

(b) Fiber microstresses.

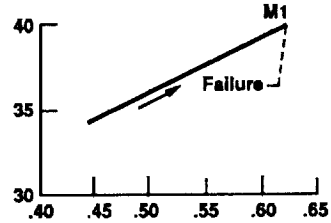

(c) Matrix microstresses in region A.

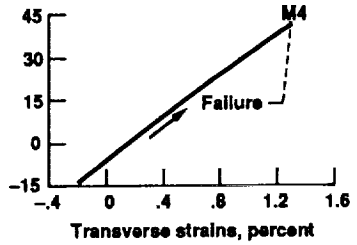

(d) Matrix microstresses in region C.

Figure 8.—Transverse stress-strain curves for middle (90°) ply and its fiber and matrix (regions A and C).

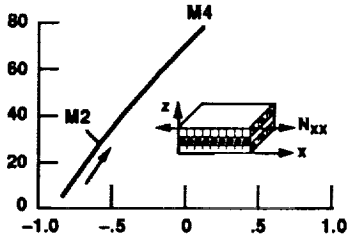

(a) Ply stresses.

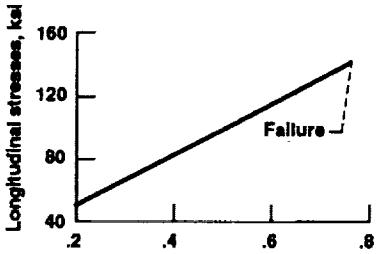

(b) Fiber microstresses.

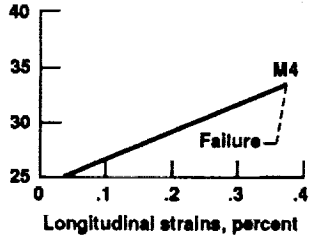

(c) Matrix microstresses in regions A and C.

Figure 9.—Longitudinal stress-strain curves for bottom (0°) ply and its fiber and matrix (regions A andC).

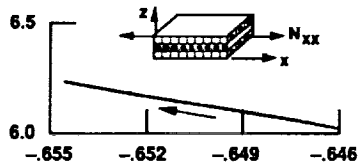

(a) Ply stresses.

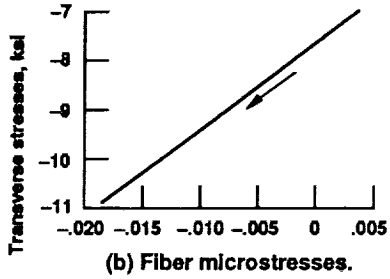

(b) Fiber microstresses.

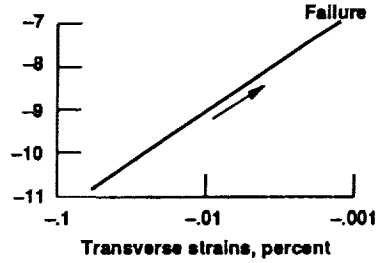

(c) Matrix microstresses in region C.

Figure 10.—Transverse stress-strain curves for bottom (0°) ply and its fiber and matrix (region C).

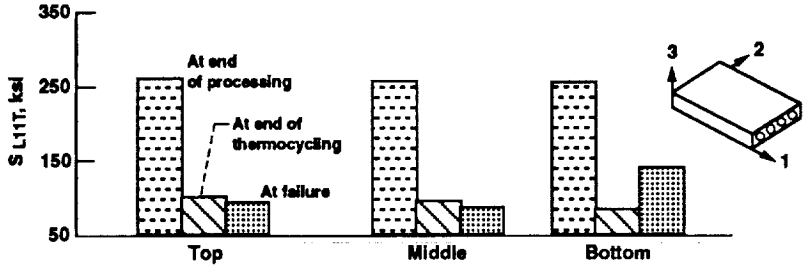

(a) Longitudinal direction (1-direction).

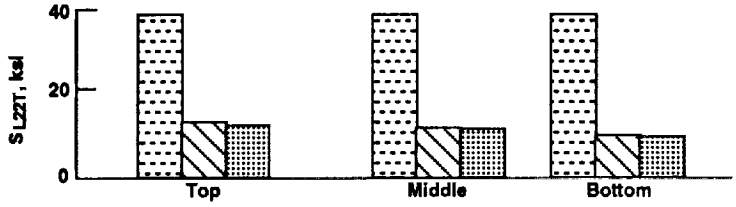

(b) Transverse direction (2-direction).

Figure 11.—Tensile strength for different plies.

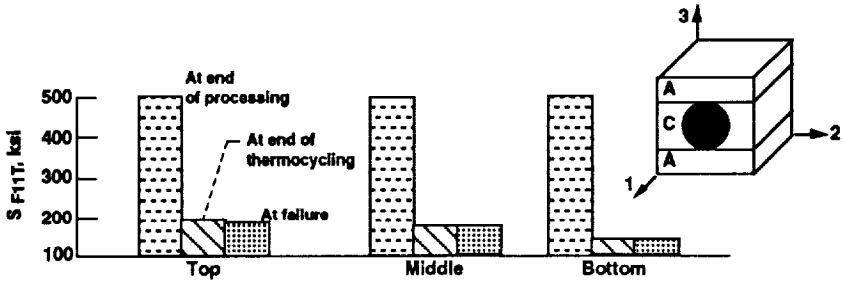

(a) Fiber tensile strength in longitudinal direction (1-direction).

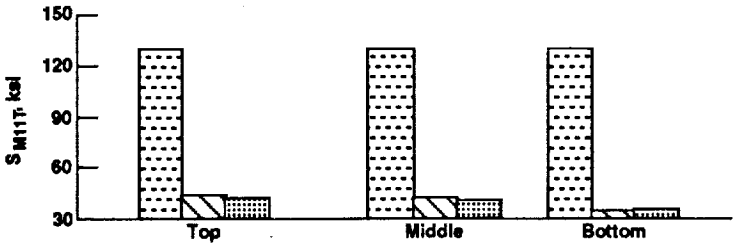

(b) Matrix tensile strength in longitudinal direction (1-direction).

Figure 12.—Longitudinal tensile strength for fiber and matrix of different plies.

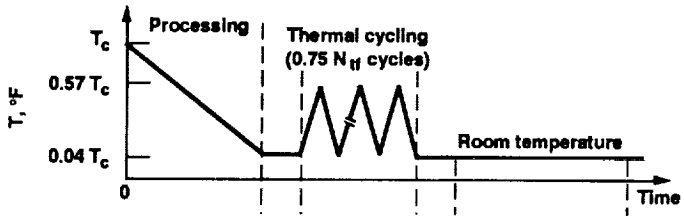

(a) Thermal load. T_c = 1750 °F.

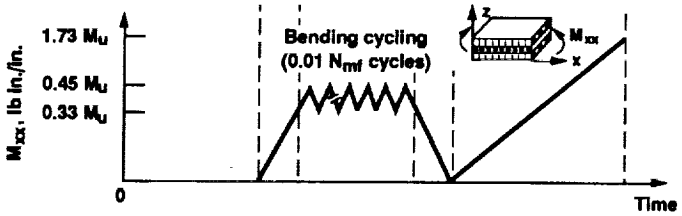

(b) Bending load. M_u = 866.67 lb in./in.

Figure 13.—Second case of loading.

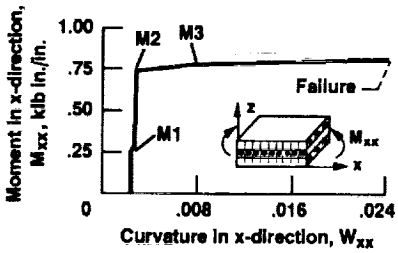

Figure 14.—Moment versus curvature.

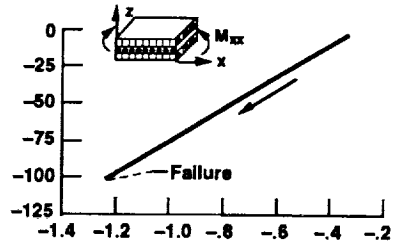

(a) Ply stresses.

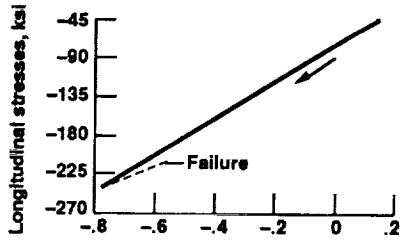

(b) Fiber microstresses.

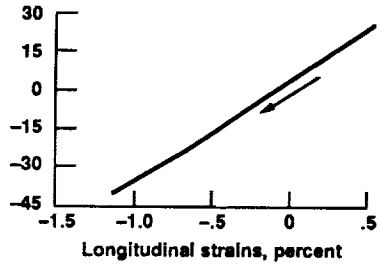

(c) Matrix microstresses in regions A and C.

Figure 15.—Longitudinal stress-strain curves for top (0°) ply and its fiber and matrix (regions A and C).

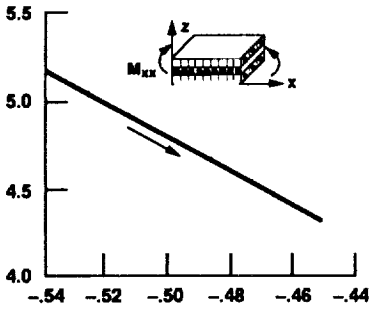

(a) Ply stresses.

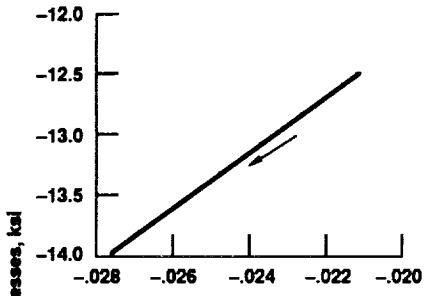

(b) Fiber microstresses.

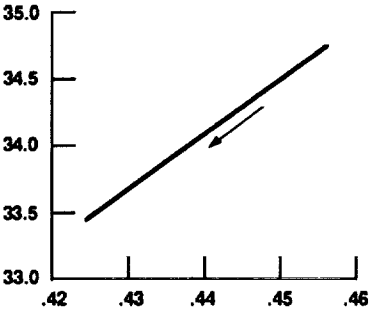

(c) Matrix microstresses in region A.

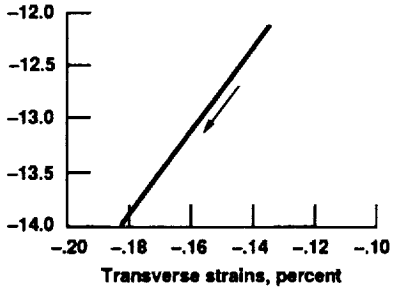

(d) Matrix microstresses in region C.

Figure 16.—Transverse stress-strain curves for top (0°) ply and its fiber and matrix (regions A and C).

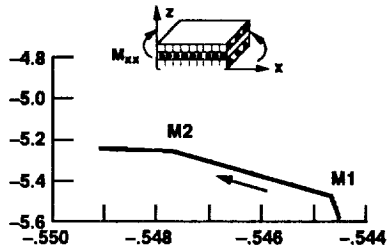

(a) Ply stresses.

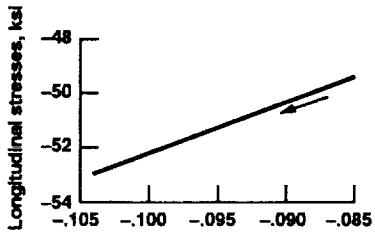

(b) Fiber microstresses.

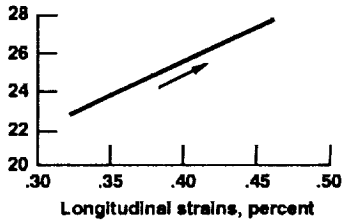

(c) Matrix microstresses in regions A and C.

Figure 17.—Longitudinal stress-strain curves for middle (90°) ply and its fiber and matrix (regions A and C).

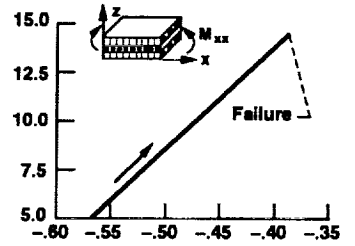

(a) Ply stresses.

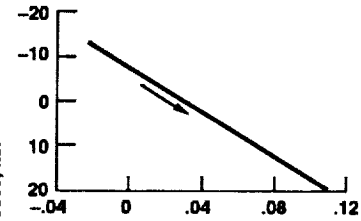

(b) Fiber microstresses.

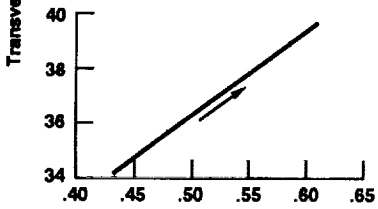

(c) Matrix microstresses in region A.

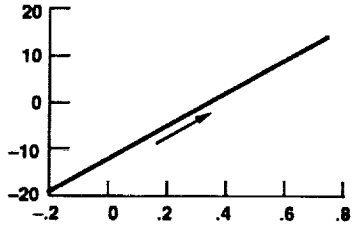

(d) Matrix microstresses in region C.

Figure 18.—Transverse stress-strain curves for middle (90°) ply and its fiber and matrix (regions A and C).

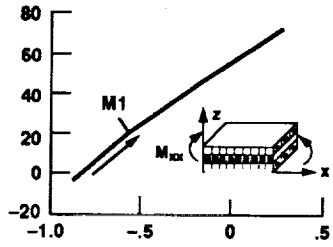

(a) Ply stresses.

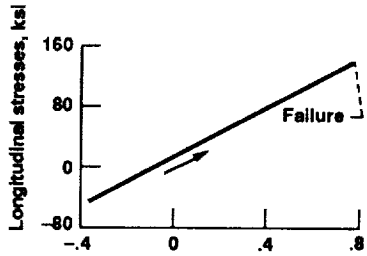

(b) Fiber microstresses.

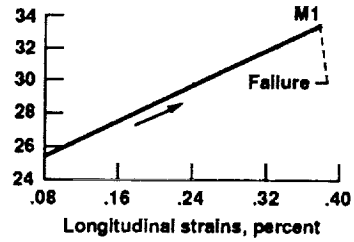

(c) Matrix microstresses in regions A and C.

Figure 19.—Longitudinal stress-strain curves for bottom (0°) ply and its fiber and matrix (regions A and C).

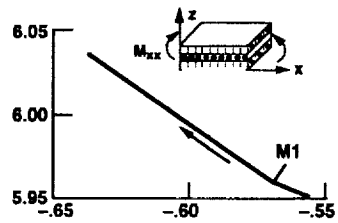

(a) Ply stresses.

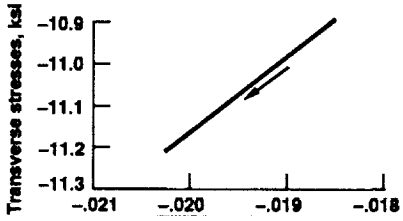

(b) Fiber microstresses.

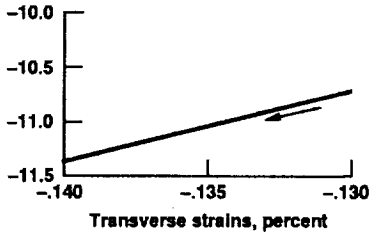

(c) Matrix microstresses in region C.

Figure 20.—Transverse stress-strain curves for bottom (0°) ply and its fiber and matrix (region C).

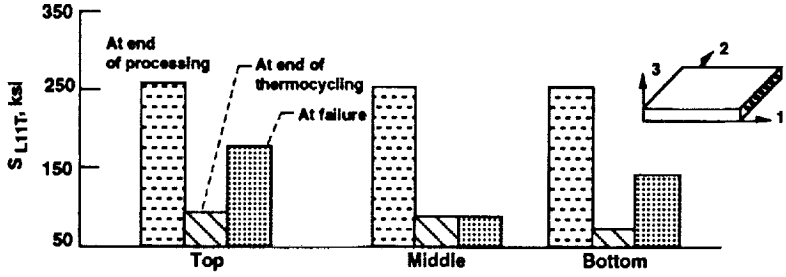

(a) Longitudinal direction (1-direction).

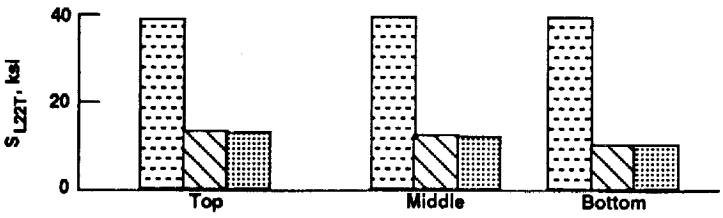

(b) Transverse direction (2-direction).

Figure 21.—Tensile strength for different plies.

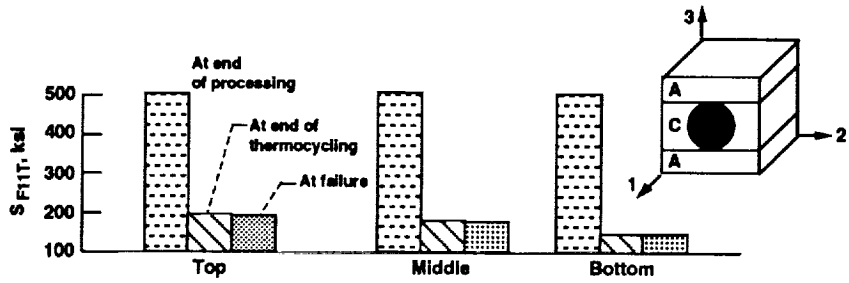

(a) Fiber tensile strength in longitudinal direction (1-direction).

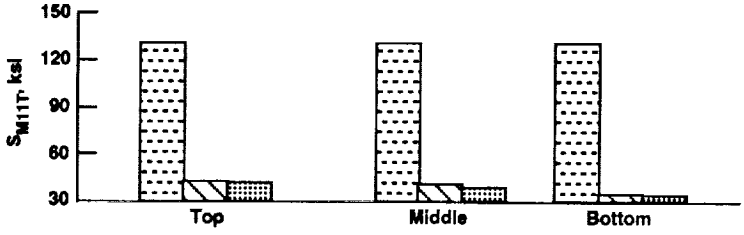

(b) Matrix tensile strength in longitudinal direction (1-direction).

Figure 22.—Longitudinal tensile strength for fiber and matrix of different plies.

NASA
National Aeronautics and Space Administration

Report Documentation Page

1. Report No.	2. Government Accession No.	3. Recipient's Catalog No.
NASA TM - 104354		

4. Title and Subtitle
Combined Thermal and Bending Fatigue of High-Temperature Metal-Matrix Composites: Computational Simulation

5. Report Date
June 1991

6. Performing Organization Code

7. Author(s)
Pascal K. Gotsis

8. Performing Organization Report No.
E - 6140

10. Work Unit No.
510 - 10 - 01

9. Performing Organization Name and Address
National Aeronautics and Space Administration
Lewis Research Center
Cleveland, Ohio 44135 - 3191

11. Contract or Grant No.

13. Type of Report and Period Covered
Technical Memorandum

12. Sponsoring Agency Name and Address
National Aeronautics and Space Administration
Washington, D.C. 20546 - 0001

14. Sponsoring Agency Code

15. Supplementary Notes
Responsible person, Pascal K. Gotsis, (216) 433 - 3331.

16. Abstract

The nonlinear behavior of a high-temperature metal-matrix composite (HT-MMC) was simulated by using the METCAN (Metal Matrix Composite Analyzer) computer code. The simulation started with the fabrication process, proceeded to thermomechanical cyclic loading, and ended with the application of a monotonic load. Classical laminate theory and composite micromechanics and macromechanics are used in METCAN, along with a multifactor interaction model for the constituents' behavior. The simulation of the stress-strain behavior from the macromechanical and the micromechanical points of view, as well as the initiation and final failure of the constituents and the plies in the composite, was examined in detail. It was shown that, when the fibers and the matrix were perfectly bonded, the fracture started in the matrix and then propagated with increasing load to the fibers. After the fibers fractured, the composite lost its capacity to carry additional load and fractured.

17. Key Words (Suggested by Author(s))	18. Distribution Statement
Metal-matrix composite; Nonlinear behavior; High temperature; Thermal/bending cycling; Stress-strain curves; Fractures (materials); Evolution (fracturing)	Unclassified - Unlimited Subject Category 24

19. Security Classif. (of the report)	20. Security Classif. (of this page)	21. No. of pages	22. Price*
Unclassified	Unclassified	24	A03

NASA FORM 1626 OCT 86

*For sale by the National Technical Information Service, Springfield, Virginia 22161